Journal of ELECTRONIC MATERIALS, Vol. 40, No. 9, 2011
DOI: 10.1007/s11664-011-1672-3
© 2011 TMS

Evaluation of Electrochemical Migration on Printed Circuit Boards with Lead-Free and Tin-Lead Solder

XIAOFEI HE,[1] MICHAEL H. AZARIAN,[1] and MICHAEL G. PECHT[1,2]

1.—Center for Advanced Life Cycle Engineering, University of Maryland, College Park, MD 20742, USA. 2.—e-mail: pecht@calce.umd.edu

To evaluate the current leakage and electrochemical migration behavior on printed circuit boards with eutectic tin-lead and lead-free solder, IPC B-24 comb structures were exposed to 65°C and 88% relative humidity conditions under direct-current (DC) bias for over 1500 h. These boards were processed with either Sn-3.0Ag-0.5Cu solder or Sn-37Pb solder. In addition to solder alloy, board finish (organic solderability preservative versus lead-free hot air solder leveling), spacing (25 mil versus 12.5 mil), and voltage (40 V versus 5 V bias) were also assessed by using *in situ* measurements of surface insulation resistance (SIR) and energy-dispersive spectroscopy after testing. It was shown that an initial increase of SIR was caused by consumption of electroactive species on the surface, intermittent drops of SIR were caused by dendritic growth, and a long-term SIR decline was caused by electrodeposition of a metallic layer. The prolonged SIR decline of Sn-3.0Ag-0.5Cu boards was simulated by three-dimensional (3D) progressive and instantaneous nucleation models, whose predictions were compared with experimental data. Sn-37Pb boards exhibited comigration of Sn, Pb, and Cu, while Sn-3.0Ag-0.5Cu boards incurred comigration of Sn, Ag, and Cu. Among the migrated species, Sn always dominated and was observed as either a layer or in polyhedral deposits, Pb was the most common element found in the dendrites, Cu was a minor constituent, and Ag migrated only occasionally. Compared with solder alloy, board finishes played a secondary role in affecting SIR due to their complexation with or dissolution into the solder. The competing effect between electric field and spacing was also investigated.

Key words: Electrolyte, electrochemical migration, dendrite, current leakage, surface insulation resistance, reliability

INTRODUCTION

The current trend of electronic products is toward high-density packaging, high circuit speeds, and high input and output counts.[1] This requires miniaturization of electronic components and reduction of spacing on printed circuit boards (PCBs). The typical spacings in dual-in-line (DIL) packages 20 years ago were 2.54 mm (0.1 inch),[2] but nowadays the spacings associated with some surface-mount technology (SMT) circuits are between 0.1 mm and 0.25 mm (4 mil to 10 mil).[3] This shrinkage of spacing between biased metallizations, together with moisture adsorption and contaminants on PCBs,[1] can trigger an electrochemical phenomenon[4–8] called electrochemical migration (ECM), which is the growth of metallic dendritic structures across the gap between electrodes in the presence of moisture under a DC bias. If a dendritic structure bridges the gap, an electrical short can occur. At constant voltages, a reduction of spacing on a PCB will increase the electric field and shorten the migration distance, which will decrease the time to failure and thus increase the reliability risk for electronic products.

The occurrence of ECM requires a DC voltage, an electrolyte, and metal ions. The electrolyte can be

(Received August 25, 2010; accepted May 12, 2011; published online June 15, 2011)

either adsorbed moisture films on the substrate or condensed droplets of water. In the case of moisture adsorption, the maximum number of adsorbed monolayers of water at a certain temperature cannot be infinite; for example, at 23°C and 100% relative humidity (RH), polytetrafluoroethylene can adsorb 3 monolayers at most, quartz can adsorb a maximum of 7 monolayers,[9] but for α-alumina, the maximum number of adsorbed monolayers is around 25.[10] On PCBs at 40°C/93% RH or 85°C/85% RH, a typical adsorbed moisture layer is many nanometers in thickness.[11] Due to the interaction between the substrate and the adsorbed moisture, the first few layers do not behave like bulk water. Only when the number of monolayers of adsorbed moisture is above a critical value can the successive adsorbed layers start to behave as bulk water.[9,10] Migrating metal ions can originate from metallization (copper traces), finish (such as immersion tin, silver, etc.), or solder (such as Sn-Pb, Sn-Ag-Cu, or similar alloy systems).

The ECM process consists of the following sequence of steps: path formation, electrodissolution, ion transport, electrodeposition, and filament growth.[12] Path formation is the creation of a favored path—a medium consisting of an electrolyte layer for metal ions to migrate. Electrodissolution involves the oxidation of metals to generate cations at the anode. These cations tend to migrate under the influence of electromotive forces to the cathode (ion transport) and deposit there as neutral metal (electrodeposition). As more and more neutral metals deposit on the nuclei, a dendritic structure may grow and propagate from cathode to anode (filament growth).

Typical accelerated test conditions for ECM on PCBs involve the exposure of test specimens to elevated temperature, humidity, and voltage bias (THB) levels, which are intended to reduce the time to failure without inducing condensation.[13] The contributions of material and processing factors to ECM in THB conditions, such as conformal coating, flux, conductor spacing, and voltage bias, have been reported previously.[12]

Over the past several years, lead-free solder alloys have been widely used as a replacement for traditional eutectic tin-lead solder. Although some studies have been published on the relative risk of ECM with selected lead-free solder alloys and finishes,[14,15] there are few reported results from THB tests which compare tin-lead and Sn-Ag-Cu solder alloys. This paper is intended to compare the differences in electrical and electrochemical behaviors of Sn-37Pb (SnPb) and Sn-3.0Ag-0.5Cu (SAC) soldered PCBs subjected to THB exposure. The surface insulation resistance (SIR) trends and the morphologies of migrated metals were analyzed. In addition to solder alloy, board finish, electric field, and conductor spacing were also investigated with respect to their contributions to ECM.

EXPERIMENTAL PROCEDURES

An IPC B-24 board with interleaved comb structures was chosen and modified for this study. Since the 16 mil and 20 mil spacings used on the IPC B-24 board have little difference in either migration distance or electric field for the same voltage, 12.5 mil (0.32 mm) and 25 mil (0.64 mm) spacings were adopted to further differentiate spacing effects.

A typical lead-free solder, SAC solder, was chosen to compare with the traditional eutectic SnPb solder with respect to their susceptibility to ECM. Each was reflow-soldered onto copper comb structures to create samples on which the migrating species, morphologies, and metallic distributions could be compared. Prior to soldering, the copper traces were finished with either organic solderability preservative (OSP) or lead-free hot air solder leveling (HASL), to compare a relatively low-cost organic finish (OSP) with one type of inorganic finish (HASL). Thus the comparisons included: SnPb versus SAC solder, OSP versus HASL finishes, and 0.32 mm (12.5 mil) versus 0.64 mm (25 mil) conductor spacings. Figure 1 shows the test specimens.

No-clean fluxes were used in the reflow solder paste, since no-clean flux is now widely used in the electronics industry. REL0 flux was used in the SnPb solder paste and ROL0 flux was used in the SAC solder paste. Based on the notation for solder fluxes given in IPC-J-STD-004,[16] "RE" and "RO" designate resin and rosin, respectively. "L" indicates low activity, and "0" means that the halide content is below 0.05% in the flux residue.

Fig. 1. Image of a test board prior to soldering, containing comb structures based on an IPC B-24 pattern, with 0.64 mm (25 mil, left) and 0.32 mm (12.5 mil, right) conductor spacings.

The temperature and humidity conditions (65°C/88% RH) were selected based on the recommendations of IPC-TM-650 method 2.6.14.1. Since prior studies[12] showed that testing at higher temperatures (such as 85°C) can cause the weak organic acids in no-clean fluxes to be volatilized, the choice of a higher temperature could have adversely affected the usefulness of the test results, since field conditions typically involve lower temperatures. Thus 65°C was chosen as the test temperature. The test humidity (88% RH) is within the range of humidities (85% to 93% RH) commonly used in THB tests. While the IPC standard calls for a 500 h test duration, longer test times were selected for this study because the major objective was to provide insights that would be of general relevance to electronic products, including those with an expected life of more than just a few years, rather than simply qualifying a candidate process to a minimum requirement. The actual test durations were 1653 h for the 40 V test and 1550 h for the 5 V test. The voltage biases selected were 40 V and 5 V DC so as to cover a range of voltages that may be used in power lines and signal lines. The SIR failure threshold was 100 MΩ, consistent with the criteria cited in IPC J-STD-004A method 3.4.5.1 and IPC-9201. For each combination of experimental factors, 3 identical test comb structures were tested, so in total 24 comb structures were tested at each of two voltages. Table I provides an overview of the test matrix.

An SIR test system was used to detect leakage current. The SIR test system comprised a computer, a high-resistance meter, low-noise switches, a temperature–humidity chamber, a DC power supply, triax cabling, and the test boards. The multichannel high-resistance meter was an Agilent 4349B with measurement range from 10^3 Ω to 10^{15} Ω. Its accuracy ranges from 2.5% to 3.1%. Agilent E5252A low-noise switches provided the ability to multiplex 48 channels to the resistance meter, allowing an SIR reading to be collected once every 3.6 min for each comb pattern. A 1 MΩ current-limiting resistor was placed in series with each comb pattern to minimize fusing of dendrites in the event of a drop in SIR, while still providing the opportunity to observe SIR behavior over about four orders of magnitude in resistance.

Table I. THB test board characteristics and process factors

Solder alloy	SnPb, SAC
Solder process	Reflow
Board finish	OSP, lead-free HASL
Conductor spacing	0.32 mm (12.5 mil), 0.64 mm (25 mil)
Voltage bias	5 V, 40 V
Flux (no clean)	ROL0 for SAC, REL0 for SnPb
Substrate	FR-4 (170°C glass-transition temperature)
Replicates	3
Environment	65°C/88% RH (noncondensing)
Duration	1653 h for 40 V, 1550 h for 5 V

RESULTS AND DISCUSSION

The times to failure of SIR data collected during the THB tests (40 V and 5 V) are shown in Tables II and III.

SIR Behavior of Solder Alloy: SnPb Versus SAC

The experimental results (Tables II, III) reveal that the SnPb boards consistently incurred fewer failures than the SAC boards. The switch from 40 V to 5 V led to an appreciable decrease in the number of failures on the SnPb boards, while this switch did not greatly affect the number of failures on the SAC boards. Given the same finish or spacing, the number of failures of the SnPb boards was always lower than that on the SAC boards. In addition, the times to failure of the SnPb boards had greater variability compared with the more narrowly

Table II. Times to failure for comb structures on PCBs biased at 40 V in 65°C/88% RH

			Time to Failure (h)		
Solder	Finish	Spacing (mil)	Sample 1	Sample 2	Sample 3
SnPb	OSP	25	s	s	s
		12.5	1313.8	0	195.7
	HASL	25	s	s	s
		12.5	1.4	9.4	s
SAC	OSP	25	1063.4	s	888.6
		12.5	85.6	87.3	91.3
	HASL	25	706.3	257.8	1365.9
		12.5	117.6	134.4	101.7

"s" means survived.

Table III. Times to failure for comb structures on PCBs biased at 5 V in 65°C/88% RH

			Time to Failure (h)		
Solder	Finish	Spacing (mil)	Sample 1	Sample 2	Sample 3
SnPb	OSP	25	s	s	s
		12.5	s	s	s
	HASL	25	s	s	s
		12.5	234	s	s
SAC	OSP	25	s	s	s
		12.5	432.1	539.8	353.9
	HASL	25	s	900	871.9
		12.5	423.6	273.3	409.6

"s" means survived.

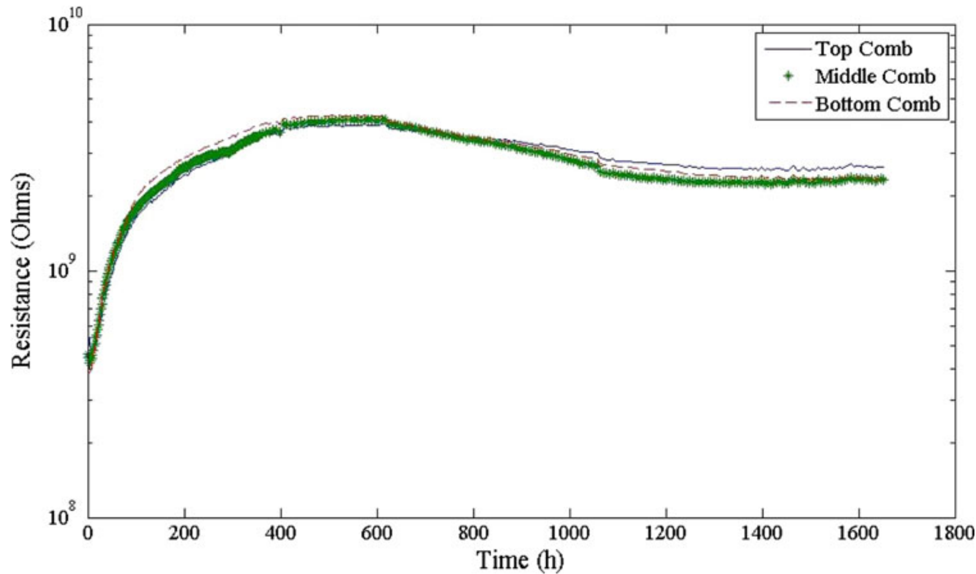

Fig. 2. Results for 40 V SIR of three comb structures on a SnPb soldered board with HASL finish and 25 mil spacing. Top comb, middle comb, and bottom comb are simply a means of distinguishing the comb structures according to their location on the board.

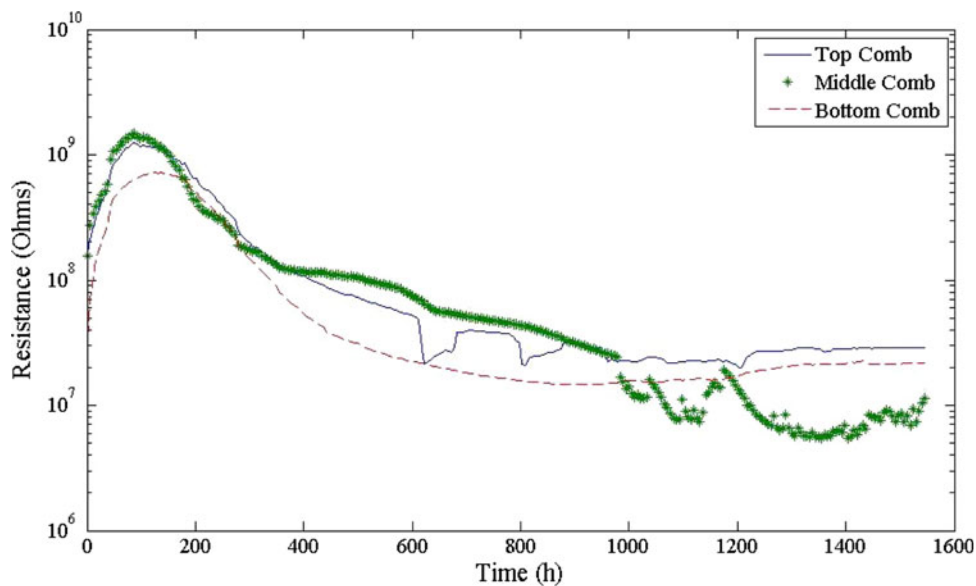

Fig. 3. Results for 5 V SIR of three comb structures on a SAC soldered board with OSP finish and 12.5 mil spacing.

distributed times to failure of SAC boards, for the same finish and spacing.

The SIR trends between SnPb soldered and SAC soldered samples were different, as shown in Figs. 2 and 3. The SIR of the SnPb samples showed an increasing trend in the beginning of the test, followed by a gradual leveling off. The SIR of the SAC samples, however, showed a long-term decline after increasing for an initial period of about 100 h. This phenomenon occurred for all SnPb and SAC boards in both 40 V and 5 V THB tests, regardless of which types of finish and spacing were used.

The long-term behavior of SnPb and SAC boards can be explained as follows. Initially, after the humidity and bias were applied, the adsorbed moisture films on the FR-4 laminate surface combined with flux residues and ionic contaminants on the PCB surface to build up an electrolyte. Flux residue contains organic salts (fluxing product) and weak organic acids (remaining flux activators) such as adipic and glutaric acids, which are the common activators of no-clean flux. Together with the DC bias between electrodes, an electrochemical cell is formed.

Analysis of SIR curves of surviving SnPb samples shows that the relationship between SIR, R, and time, t, follows a power law $R = at^n$, where a is a constant. Averaged R^2 values, a measure of the goodness of fit, were 0.98 for 40 V SIR curves and

0.92 for 5 V SIR curves, indicating that the fits were good. The n values of 40 V stressed samples ranged from 0.40 to 0.67, with a mean of 0.52. The n values of 5 V stressed samples ranged from 0.43 to 0.72, with a mean of 0.61. A t-test (statistical hypothesis test) was conducted, and it was found that there was no statistical difference between the means of these two groups of n values when a significance level of 5% was applied. Thus, it is unlikely that n is voltage dependent. Taking into account the experimental statistical uncertainties, it is most likely that the mean value of n is between 0.5 and 0.6. This suggests that the SIR of the comb structure is approximately proportional to the square root of time, which is a typical characteristic of a diffusion-controlled ion transport process under constant voltage.[17,18]

The initial SIR increase on SnPb boards implies an initial current decay with time. Surface current decay on a polymer under constant voltage has been investigated for several decades. The polymers studied include epoxy resin,[19,20] polytetrafluoroethylene,[9] polyethylene,[21] polypropylene,[22] poly(hexafluoropropylene-tetrafluoroethylene),[23] etc. The relation between the current I, the so-called absorption current, and time t is described as $I \propto t^n$. When the polymer is tested in vacuum, n is close to -1, whilst in air, n is between -0.6 and -0.8.[22–24] Thus, the absorption current decays more slowly in air than in vacuum. Explanations for this absorption current decay include lateral spread of surface charges in vacuum,[24] polymer surface polarization,[25] charge injection,[26] and electron hopping across surface-localized states.[27] The polymers mentioned above are cleaned polymers, but for epoxy resin, especially with ionic contaminants on the surface, this current decay has been attributed to a diffusion-controlled process and analyzed in the *frequency* domain.[19] Unfortunately, the origin of charge carriers has not been exactly specified. The charge carriers can be electrons,[27] most likely in vacuum, but in air when moisture adsorption takes place it is generally accepted that the charge carriers have ionic nature.[19–22,26]

Since surface conductivity of a polymer exposed to water vapor is always several orders of magnitude higher than that in a vacuum, most likely the charge carriers with moisture adsorption present are ions. So the resistance–time transient response to the constant bias U based on ion transport in a cell is

$$R = \frac{U}{i_{\mathrm{Total}}A} = \frac{U}{\sum_1^k \left(z_i F c_i^{\mathrm{b}} (a-1) \sqrt{\frac{D_i}{\pi t}} \right) A} = \frac{U}{\sum_1^k \left(z_i F c_i^{\mathrm{b}} (a-1) \sqrt{\frac{D_i}{\pi}} \right) A} \sqrt{t}, \quad (1)$$

where A is the cross-sectional area of the electrolyte, i_{Total} is the total current density, z_i is the charge number, F is the Faraday constant, c_i^{b} is the initial bulk concentration of a specific type of electroactive ion, a is a constant determined by the system, D is the diffusivity, and t is time. A detailed derivation of Eq. (1) is given in the Appendix.

From Eq. (1) we can see that $R \propto t^{0.5}$, since z, F, a, D, A, and c_i^{b} are all constants, because the types and initial amounts of the electroactive species such as ionic contaminants were fixed after the start of the THB test. So in the initial period of time, such as the first 600 h in Fig. 2, the flux residues and ionic contaminants present on the surface of the board migrated toward the electrodes, where they were oxidized or reduced and thus consumed. Since their initial amounts on the surface were limited and fixed, their consumption on the surfaces of the electrodes created a depletion region in the vicinity of the electrodes, thus expanding the diffusion layer thickness into the bulk electrolyte with time. As more and more residues or contaminants were consumed, their concentrations in the vicinity of the electrodes decreased further, and ionic *migration* (see the Appendix) proportional to concentration decreased more and more. Ionic *diffusion* finally dominated the ion transport process on the board surface. This is true if no significant amount of metals dissolve, since the dissolution of metal can introduce new electroactive ions into the system and perturb the composition of the ionic flux, thus significantly changing the current density. On most of the survived SnPb soldered boards, little dendritic growth occurred, thus corroborating the assumption that existing flux residues and contaminants were the *only* available electroactive species in the cell.

In contrast, the SAC board did not grow dendrites, but exhibited the deposition of layers, as shown in Figs. 4 and 5. In the figures, energy-dispersive spectroscopy (EDS) maps show that migrated Sn has formed a continuous layer spreading across the gap. This indicates that electrocrystallization into a layer or film-like deposit rather than dendrites, corresponding to a nucleation and growth model, occurred.

The current–time transients of electrocrystallization in an electrochemical cell under constant voltage have been investigated previously.[28–30] Armstrong et al.[28] introduced a three-dimensional nucleation and growth model using lattice incorporation and described the current–time transient for constant DC bias (as in a potentiostat) in growing deposits of layers. For progressive 3D nucleation, where nucleation and growth of the lattice occur at the same time, the current density is

$$i = zFk_1 \left(1 - \exp\left(-\frac{\pi M^2 \gamma k_2^2}{3\rho_{\mathrm{d}}^2} t^3 \right) \right),$$

and thus the resistance is

$$R = \frac{U}{zFk_1 \left(1 - \exp\left(-\frac{\pi M^2 \gamma k_2^2}{3\rho_{\mathrm{d}}^2} t^3 \right) \right) A}. \quad (2)$$

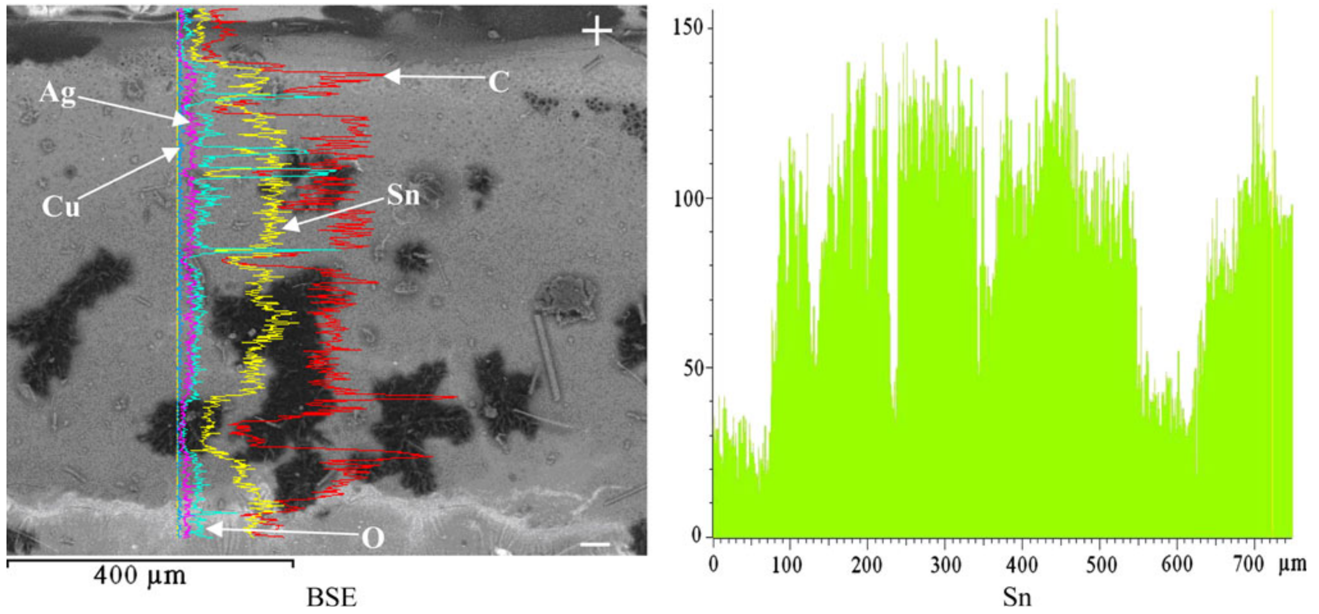

Fig. 4. EDS line scan of materials existing in the gap on a SAC soldered board with OSP finish and 25 mil spacing after 40 V THB test. The left graph is the original back-scattered electron (BSE) image, and the right graph is the Sn distribution along the line scan from the top to the bottom.

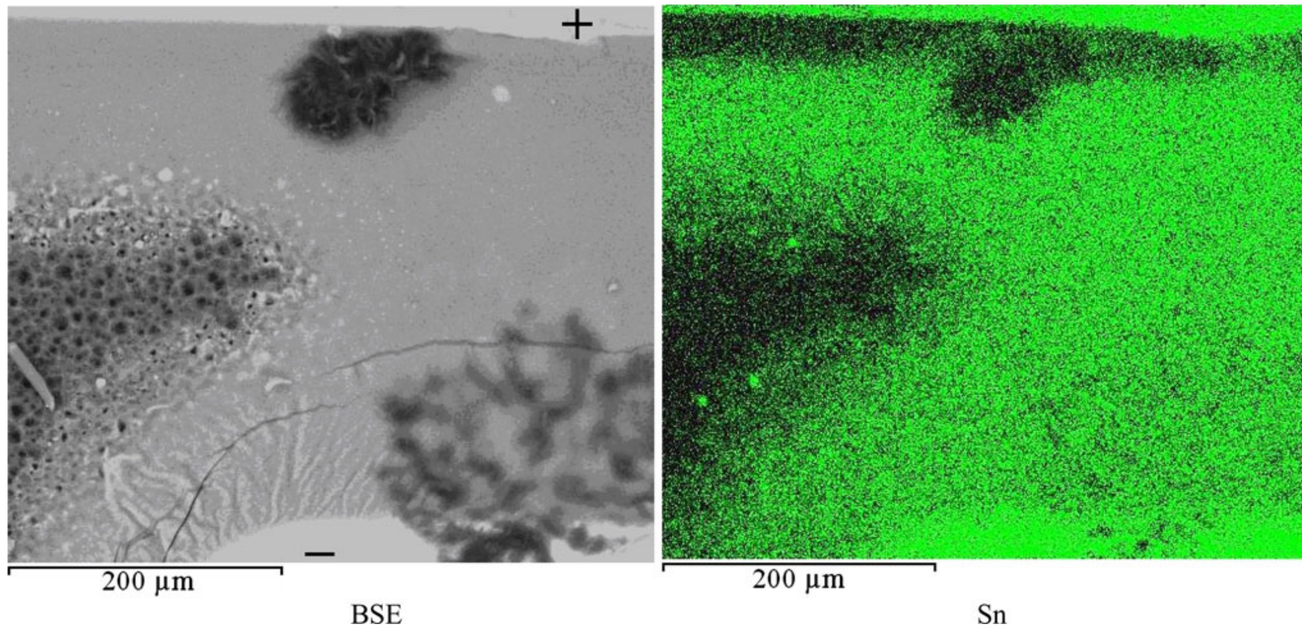

Fig. 5. EDS map of a 12.5 mil sample on a SAC soldered board with HASL finish after a 5 V THB test. The left graph is the original BSE image, and the right graph is the Sn distribution spanning the gap as a layer deposit.

For instantaneous 3D nucleation, where nucleation stops and growth of the lattice continues on the initially grown nucleation centers, the resistance is

$$R = \frac{U}{zFk_1\left(1 - \exp\left(-\frac{\pi M^2 k_2^2 N_0}{\rho_\mathrm{d}^2} t^2\right)\right)A}, \tag{3}$$

where k_1 and k_2 are the growth rate constants perpendicular and parallel to the substrate, respectively. M is the molecular weight, γ is the nucleation rate constant, N_0 is the saturation density of nuclei centers, ρ_d is the deposit density, U is the bias, t is time, and A is the cross-sectional area for the electrolyte.

Equations (2) and (3) indicate that R decreases with time and finally reaches a plateau. The final plateau is determined by k_1, the perpendicular growth rate, since the exponential terms related to k_2 and t decay with time. This suggests that, as

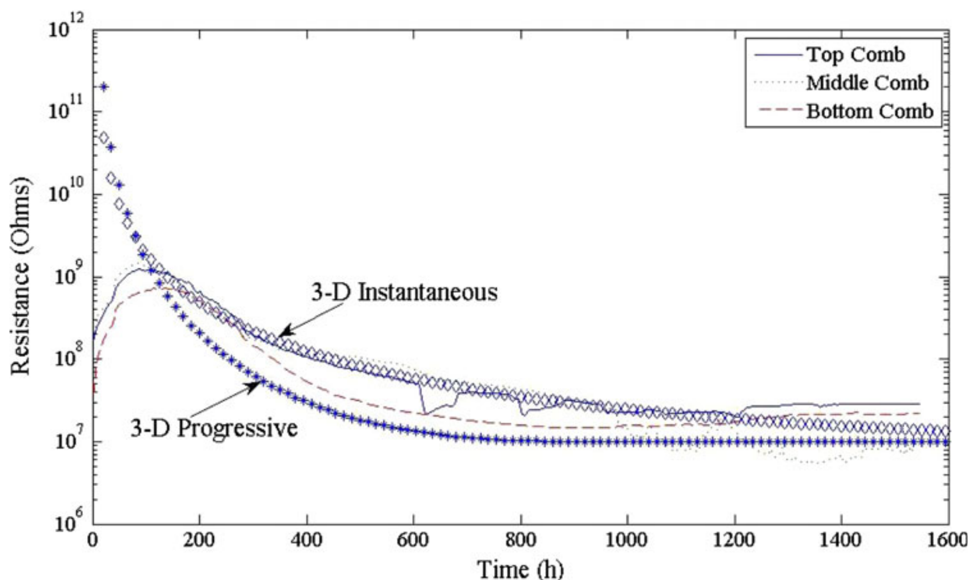

Fig. 6. Simulation of resistance with time based on Eqs. (2) and (3). The two simulated curves, for 3D progressive and instantaneous nucleation, are shown together with the experimental curves from Fig. 3.

more and more layers of deposits form at the cathode, the deposition front advances toward the anode, so the current density increases with time and the resistance decreases but eventually approaches a steady state set by k_1, the perpendicular growth rate. A simulation of the resistance–time transient based on Eqs. (2) and (3) can be made by assuming appropriate nucleation and growth rate constants for tin ions, as shown in Fig. 6. The curves in the figure were obtained under the assumptions that the electroactive species is Sn^{2+}, $k_2^2\gamma = 3 \times 10^{-22}$ mol^2 nuclei cm^{-5} s^{-3}, $k_2^2 N_0 = 3 \times 10^{-17}$ mol^2 nuclei cm^{-5} s^{-3}, $k_1 = 2.2 \times 10^{-7}$ mol cm^{-2} s^{-1}, and voltage bias $U = 5$ V. The adsorbed water layer is assumed to have a thickness of 100 nm[11] and a length of 12 mm (the length of the fingers of the comb structures), so the cross-sectional area is $A = 1.2 \times 10^{-5}$ cm^2. Note that, after 100 h, the simulated SIR curves show a long-term decline, matching the experimental data. Although it is hard to determine which type of nucleation (progressive or instantaneous) occurred on the SAC board, these two nucleation and growth models show similar SIR trends, and most likely, both types of nucleation occurred. Both the degree of matching between the SIR and the model, and the correspondence of the morphology to the model, lead to the conclusion that the SAC board experienced metal migration and deposition on the cathode as layers rather than dendrites, which generated a long-term SIR decline.

The differences in SIR behavior between SnPb and SAC boards may be caused by flux chemistry and their long-term compatibilities with solder. Both the SnPb and SAC boards contained a significant amount of flux residues before the THB tests, and flux residues spanned the gap in some places on both types of boards. The flux residues on the surface are designed either to react with water vapor or oxygen or to react at electrodes through redox reactions so that the ionic constituents of the cell are depleted with time, and thus the SIR increases to a relatively high steady value, a sign of SIR recovery. The degradation of flux residue caused by reactions between water vapor and flux or fluxing product is a diffusion-controlled process[31] characterized by diffusion of water through the outer layer of degraded flux residue to react with the inner material. Thus, the liberation of electroactive species may also be diffusion controlled, since free ions have to diffuse from inside through the outer layer of degraded flux residue to become electroactive. Either the release of electroactive species from the degraded flux residue or the consumption of electroactive species at electrodes can place the circuit under diffusion control. This is why the surviving SnPb boards without significant metal migration showed an initial diffusion-controlled SIR behavior. If, for some reason, the flux residue on the surface is not compatible with the solder in the long run, SAC solder in this case, it may complex with the solder and trigger electrochemical migration of metal ions, whose deposition as layers rather than dendrites can give rise to a long-term SIR decline. This suggests that a flux which passes standard tests (for example, 168 h at 85°C/85% RH, 96 h at 35°C/85% RH, or 96 h at 65°C/85% RH, all under bias) may not necessarily pass a THB test of more than 500 h or 1000 h.

Dendritic growth was responsible for most of the SIR failures of the SnPb boards. The dendritic growth bridging the gaps between electrodes (Figs. 8, 9) was always accompanied by intermittent SIR drops, as shown in Fig. 7. During dendritic growth, dendrites can break due to fusing[32] or

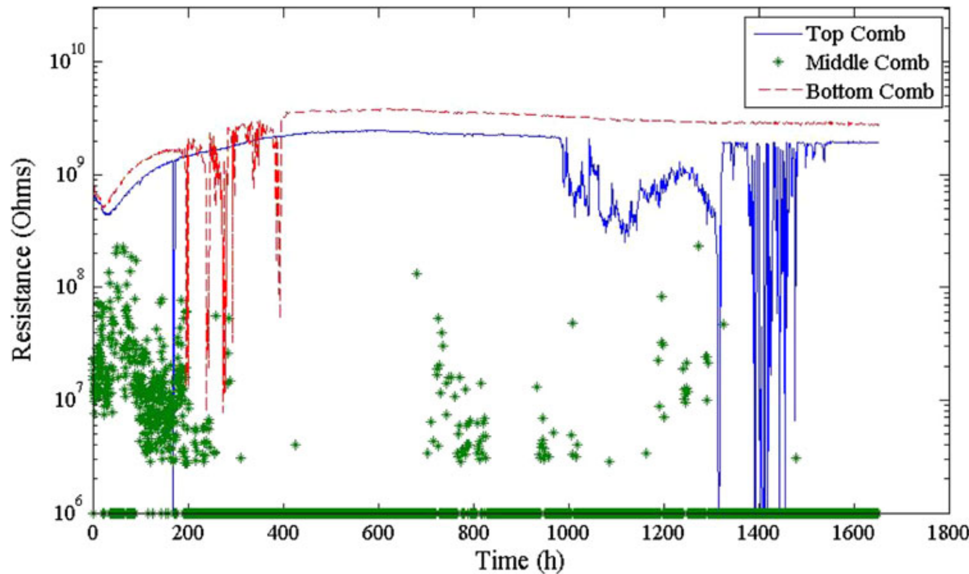

Fig. 7. Results of 40 V SIR of three comb structures on a SnPb soldered board with OSP finish and 12.5 mil spacing.

mechanical stress,[33] but rapid regrowth can occur.[33] This breaking and regrowth may cause the SIR to oscillate in a cyclic fashion and thus show intermittent drops. This is consistent with previous reports[11,34] on this phenomenon.

Morphology of Migration: SnPb Versus SAC

The morphology of electrodeposits at the cathode is affected by various factors such as the overpotential (the potential difference between the potential applied to the electrode and the potential of the electrode at equilibrium) of the cathode, current density, adhesion of nuclei to electrodes, electrolyte viscosity, and temperature. When the overpotential is small, a spongy or porous deposit can occur. When the overpotential is increased, the nucleation rate is increased, and a polycrystalline layer structure results. If the overpotential or the current density is larger than the critical values, a dendritic structure can be provoked to grow.[35]

As shown in Figs. 4 and 5, diffuse layer deposits formed on the failed SAC boards. Among the migrated species, Sn always dominated, Cu concentration was always less than Sn, and Ag was present in only small quantities and only occasionally. On failed SnPb boards, typical dendrites occurred in the 40 V THB tests (Figs. 8, 9), and polyhedral or layer-like deposits emerged in the 5 V testing (Fig. 10). Migrated Sn, Pb, and Cu coexisted in either dendrites or polyhedral deposits. In dendrites, Pb dominated, while in the polyhedral deposits, Sn dominated. Taking into account both dendrites and polyhedral deposits, Sn was still the predominant migrated species in most cases, Pb was less prevalent than Sn, and Cu was present in small proportions.

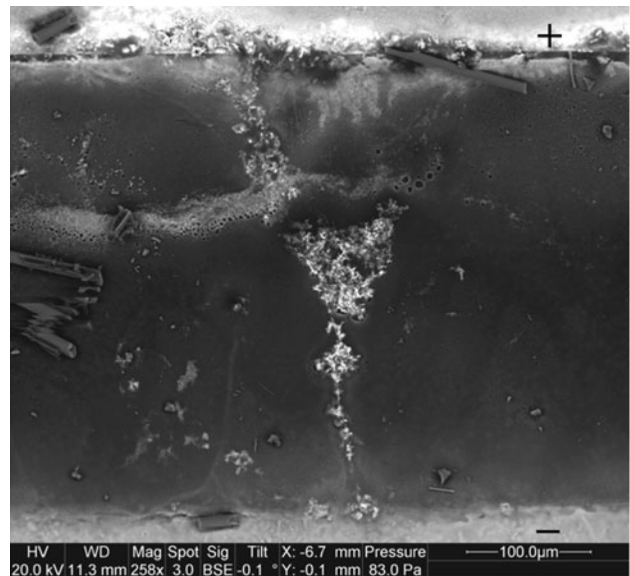

Fig. 8. Dendrite spanning the gap on a SnPb soldered board with OSP finish and 12.5 mil spacing after a 40 V THB test.

Apparently, comigration of Sn, Pb, and Cu on the SnPb board and Sn, Cu, and Ag on the SAC board occurred. Since typical cathodic overpotentials for electrodeposition of these metals are less than 1 V,[36–38] 5 V and 40 V are high in an electrodeposition sense. Assuming that the deposits were a mixture of metals in their pure states rather than solid solutions or chemical compounds, a 5 V or 40 V bias provided enough margin to accommodate the required cathodic overpotential for deposition of these metals, although the voltage drop across the surface-adsorbed film electrolyte can be significant.[11] That is why all these metals comigrated. The reason why Pb was predominant in the dendrites

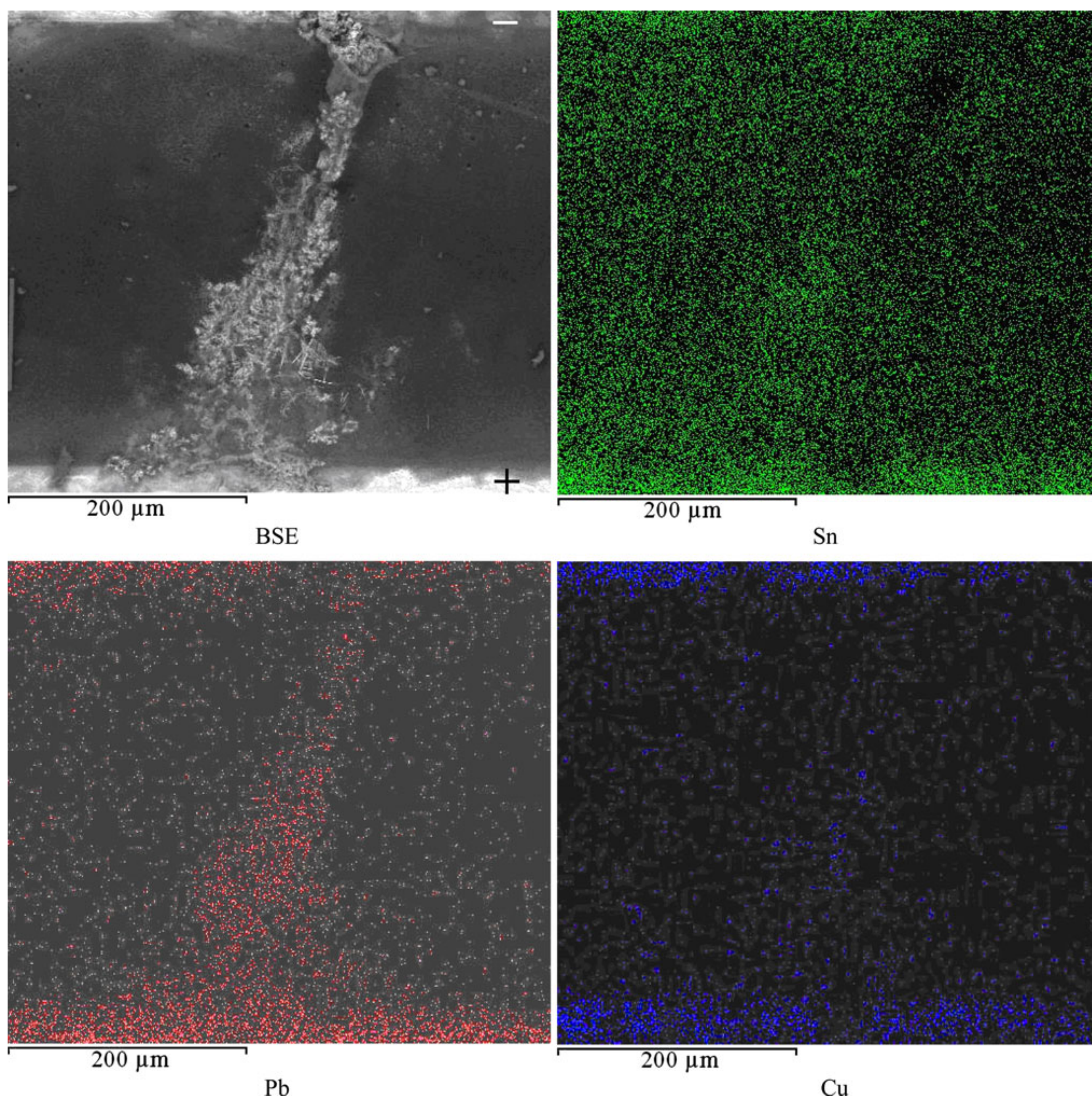

Fig. 9. BSE image and EDS map of dendrite spanning the gap on a SnPb soldered board with OSP finish and 12.5 mil spacing after a 40 V THB test.

may be due to the higher solubility of Pb^{2+} than Sn^{2+} by almost three orders of magnitude,[39] making it easier for the flux of Pb^{2+} to exceed the critical current density to trigger dendritic growth. The dominance of Sn in the overall migrated species may be due to its larger proportion in eutectic SnPb solder or SAC solder, though it had to deposit as layer structures due to the low solubility of Sn^{2+}. The reason for the occurrence of dendrites on the SnPb board in the 40 V tests was that the chance for cathodic overpotentials in the 40 V test to exceed the critical cathodic overpotential needed to trigger dendritic growth was much higher than in the 5 V test.

Effect of Board Finish: OSP Versus HASL

Finishes are used to retard the oxidation of bare copper on PCBs and maintain the solderability of metal surfaces. OSP is an organic layer evenly deposited onto exposed copper metallizations. The coating of OSP, made from benzimidazole, can be 200 nm to 500 nm thick and more durable than the previous benzotriazole version.[40] HASL involves passing boards over molten solder and blowing off excess molten solder by a hot air knife, thus leaving a thin solder layer over the exposed copper metallization. The thickness of the HASL layer can be up

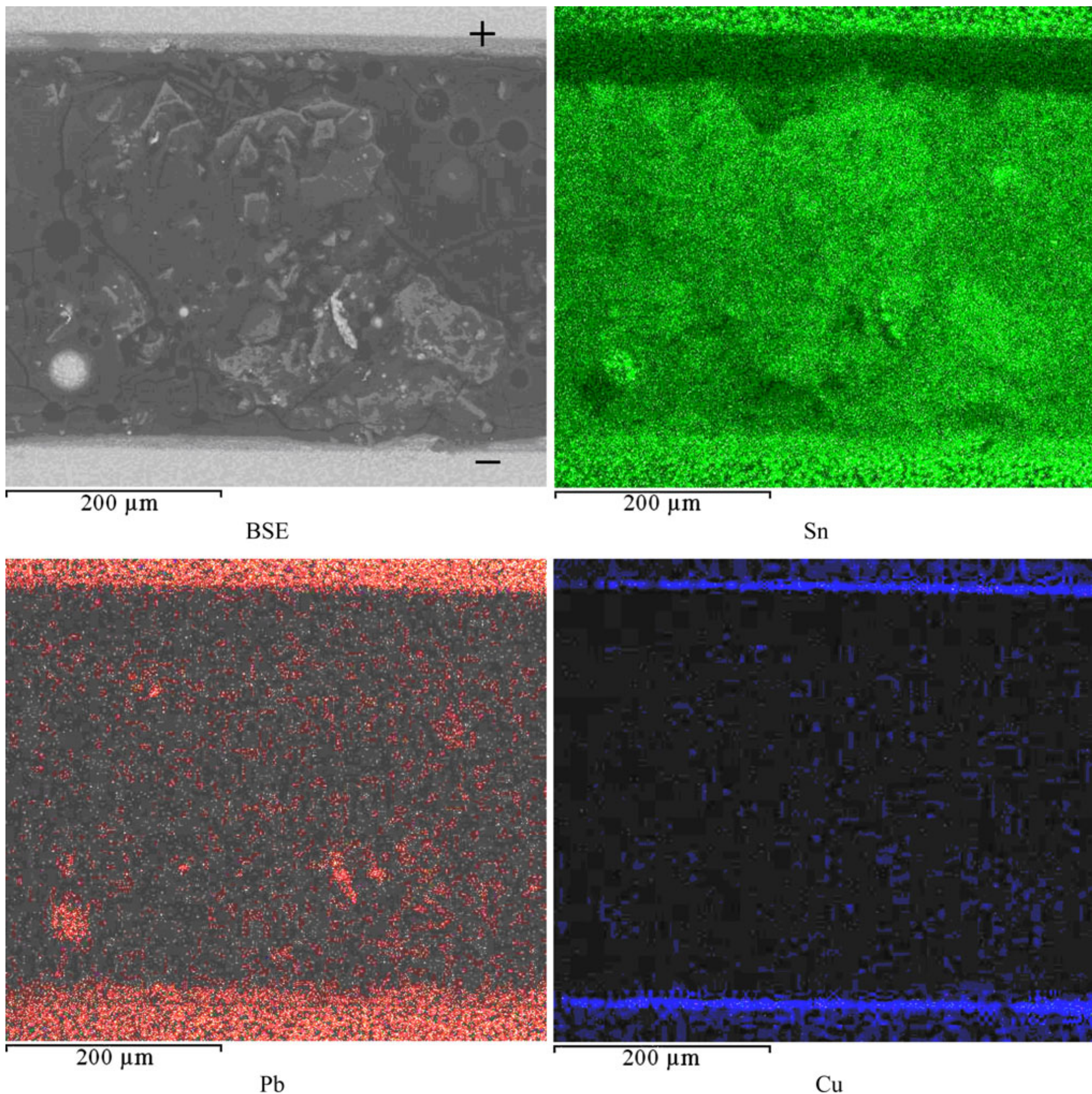

Fig. 10. Migrated metal in the shape of bumps or polyhedra on SnPb soldered board with HASL finish and 12.5 mil spacing after 5 V THB test.

to several hundred micrometers with large variations.[41] However, OSP is more prone to physical damage during PCB handling, and it can partially dissolve in solvents, including water.[40]

In the present study, OSP and HASL finishes did not show noticeable differences in their effect on SIR. This can be concluded from statistical analysis such as the Weibull analysis in Fig. 11 showing substantial overlap of the 90% confidence intervals. All boards using the same solder always showed similar SIR trends, regardless of whether OSP or HASL was used. One particular phenomenon was that OSP-finished SAC boards generated green residues, though their SIR trends were still similar to HASL-finished SAC boards.

Green residues may result from the reaction between remaining OSP and fluxing products. Benzimidazole, with a melting temperature of 170°C to 172°C,[42] may not completely evaporate during the reflow process. A green copper complex can form from the reaction between benzimidazole ligand ("HL" is the protonated form of a ligand "L") and copper sulfate at 60°C.[43] So, it is possible that the remaining OSP reacted with fluxing products (copper organic salts) and formed green residues during THB testing (65°C, 88% RH). The similar SIR trends with and

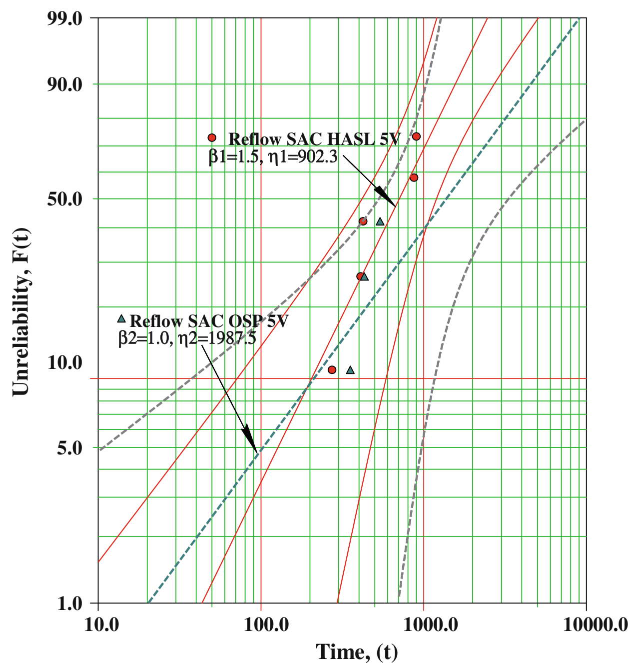

Fig. 11. Weibull plot comparing SAC soldered samples with OSP (dashed lines) and HASL finishes (solid lines) from 5 V THB test with 90% confidence intervals (CI).

without green residues suggest that green residues are not detrimental to SIR and have high resistances, thus confirming the findings of Tellefsen.[44] HASL finish can dissolve into solder during the soldering process, and therefore plays a secondary role in affecting ECM compared with solder. Thus, neither finish contributed measurably to the SIR results.

Effect of Electric Field and Spacing

Electric field acts as the driving force for ion migration. This driving force together with the relaxation effect and electrophoresis effect determines the migration velocity of ions. The relaxation effect is the overall backward drag from an ion's ionic cloud when the ion moves forward, while electrophoresis stems from the collision between ions' hydration sheaths when they move.[18] Therefore, a higher ion migration speed results from a

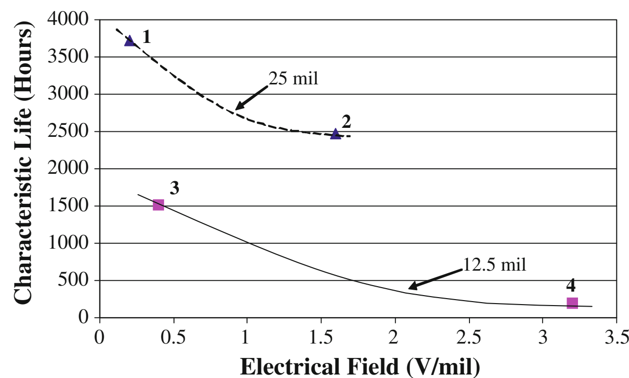

Fig. 12. Characteristic lives of four groups: 1 (0.2 V/mil, 25 mil), 2 (1.6 V/mil, 25 mil), 3 (0.4 V/mil, 12.5 mil), and 4 (3.2 V/mil, 12.5 mil). The dashed and solid curves are for illustration purposes only.

higher electric field, a higher ionic mobility, a lower electrolyte viscosity, and a smaller ionic radius (including the sheath of the ion). The spacing determines the travel distance for ions to reach the cathode and thus affects the migration time. A smaller spacing also increases the probability for flux residues or surface contaminants to bridge the gap between electrodes, allowing moisture to adsorb and form a continuous electrolyte medium (the ECM step of path formation).

Table IV presents the times to failure of different boards for four electric fields. At each value of electric field, four types of boards with the same spacing were combined into one group and the characteristic life of this group was calculated based on Weibull statistics. By doing so, four representative points were generated and are plotted in Fig. 12. One can observe that, given the same spacing, a larger electric field led to a shorter characteristic life. The combination of a larger spacing and a smaller electric field resulted in the longest characteristic life. However, a larger spacing under a higher electric field (point 2) still led to a longer characteristic life than did a smaller spacing under a lower electric field (point 3). This comparison not only suggests that spacing itself is an independent factor affecting ECM, which is consistent with the findings of Zhan et al.,[12] but it also

Table IV. Times to failure (h) of SIR according to electric field and board

Board	Electric Field (5 V, 25 mil) 0.2 V/mil	(5 V, 12.5 mil) 0.4 V/mil	(40 V, 25 mil) 1.6 V/mil	(40 V, 12.5 mil) 3.2 V/mil
SnPb_OSP	s/s/s	s/s/s	s/s/s	1313.8/0/195.7
SnPb_HASL	s/s/s	234/s/s	s/s/s	1.4/9.4/s
SAC_OSP	s/s/s	432.1/539.8/353.9	1063.4/s/888.6	85.6/87.3/91.3
SAC_HASL	s/900/871.9	423.6/273.3/409.6	706.3/257.8/1365.9	117.6/134.4/101.7

"s" means survived.

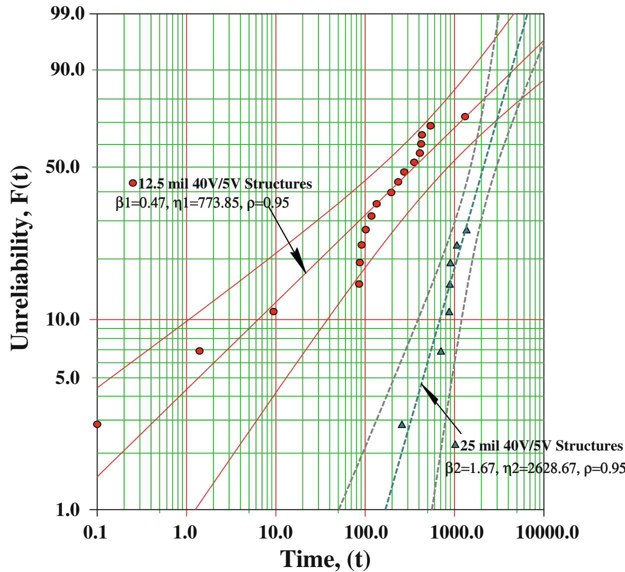

Fig. 13. Comparison between all 25 mil samples (dashed lines) and 12.5 mil samples (solid lines) from 40 V and 5 V THB tests with 90% CIs.

means that a larger spacing can overcome the disadvantageous effect induced by a larger field and still lengthen the characteristic life under some conditions. A further analysis that shows the strong effect of spacing is presented in Fig. 13, showing that a larger spacing can lengthen the characteristic life independently of electric field.

Main Effects and Interaction Effects

The main effects and interaction effects of this 2^4 (four factors, two levels) full-factorial experimental design were extracted using analysis of variance (ANOVA). It was found that greater insight into SIR response could be obtained by replacing voltage bias with electric field as a factor in the analysis. Based on the times to failure in Table IV and assuming that the failure times for the survived samples are just the termination times for the THB tests, the main effects plot and interaction plot were generated and are shown in Figs. 14 and 15. It can be observed that solder alloy and spacing are the two dominant factors, since the lines connecting their data points have steep slopes, showing larger variations from the grand mean (1000 h in this case). The electric field also shows significant influence on the SIR response. It has a similar pattern as in Fig. 12. The finish, however, does not show much influence and plays an insignificant role.

In an interaction plot, the more parallel the lines, the less interaction between the factors. The interactions between any two of these four factors, however, are not pronounced, since their lines are all more or less parallel to each other, as shown in Fig. 15. The interaction between the electric field and spacing cannot be determined from the plot due to the lack of a complete set of electric fields with one spacing, or vice versa, but their competition is discussed in the next section.

Risk Index Discussion

The observation of metal migration by itself represents a risk factor for electronic products. One way to evaluate the combined effect of metal migration and SIR degradation is to assess the metal migration and SIR with numerical values and combine them to form a risk index. The criteria are given in Table V. The final index is the sum of the risk indices of metal migration and SIR. The SIR index is the sum of the indices of the initial SIR right after temperature and humidity exposure, the

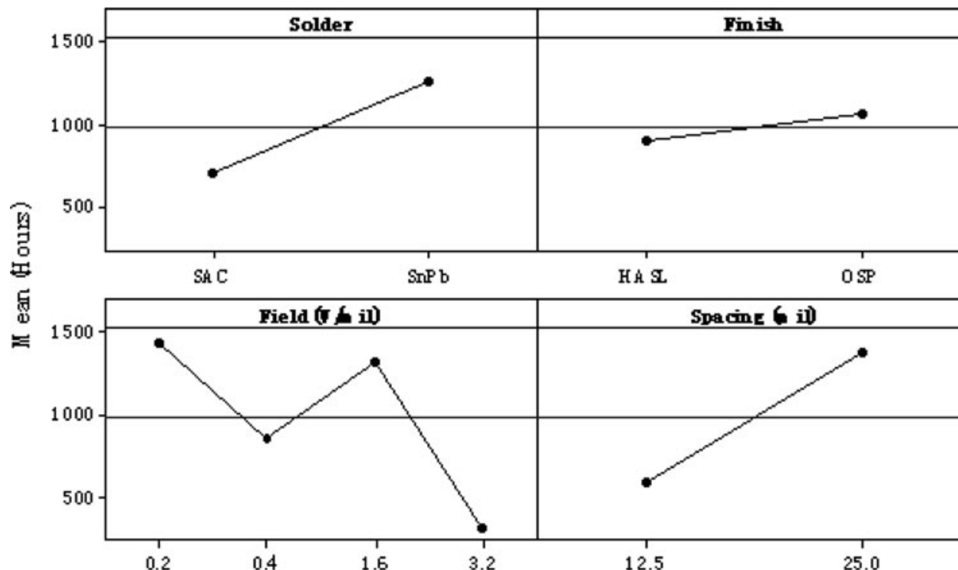

Fig. 14. Main effects plot for time to failure based on Table IV.

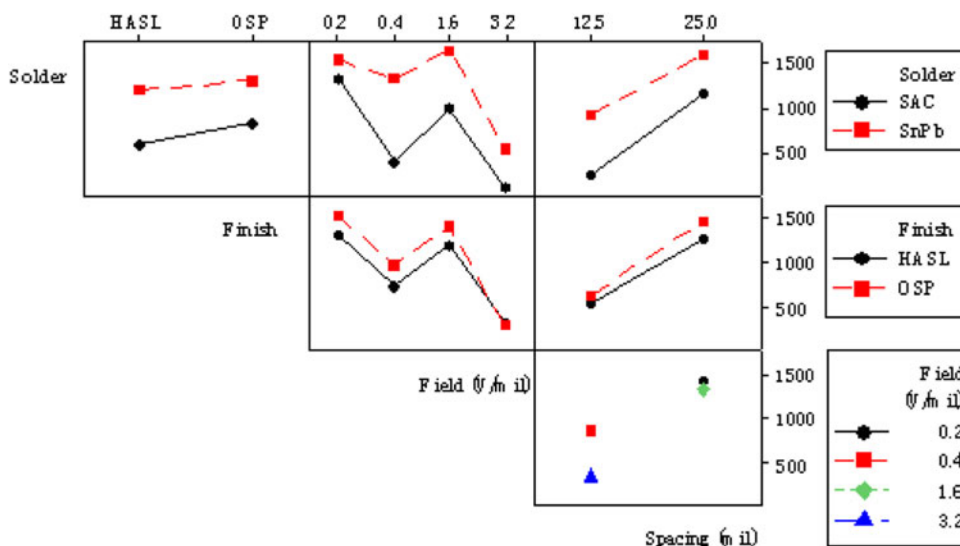

Fig. 15. Interaction plot for time to failure based on Table IV.

Table V. Risk index criteria according to metal migration and SIR degradation

Dendritic Growth (More than 20% of Conductor Spacing) or Migrated Metal Spanning the Gap	Risk Index of Metal Migration	SIR Degradation (Ω)	Risk Index of SIR
None	0	$>10^8$	0
Less than two places	1 or 2	$>10^7$	1
Few or some places	3 or 4	$>10^6$	2
Many places	5 or 6	10^6	4

SIR at 1000 h, and the final SIR of the THB test with 20%, 30%, and 50% weights associated with them, respectively.

The differences among solder alloys, finishes, and spacings with respect to their risk indexes were compared using statistical tools including fitting of distributions, means of samples, and confidence intervals. The smaller the risk index, the lower the risk associated with ECM and SIR, and the higher the reliability. From Figs. 16 and 17, it can be observed that SnPb solder has a large percentage of samples with risk indices close to zero, with its best fit being an exponential distribution. The risk index data for the SAC solder is more scattered, and the best fit is a Weibull distribution. The risk index for SnPb has a significantly smaller mean than that for SAC. OSP and HASL finishes show similar influence, since they belong to the same best-fit exponential distribution and have similar means and confidence intervals, as shown in Fig. 18.

The intervals of the risk index are plotted in Fig. 19 against an ascending series of electric fields, with an indication of their associated spacings. It can be observed that, given the same spacing, an increase in electric field increases the mean of the risk index, though this increase for 12.5 mil samples is more appreciable than for 25 mil samples.

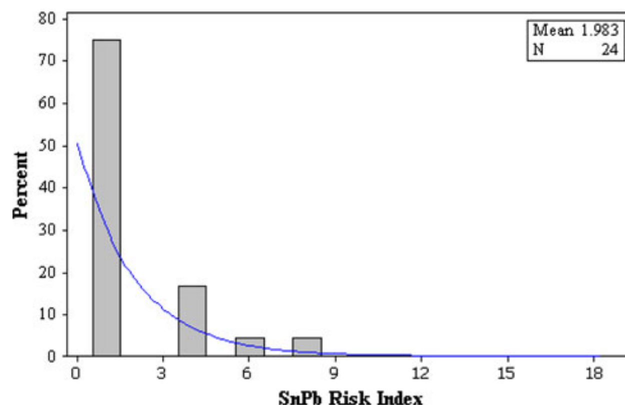

Fig. 16. Histogram of SnPb risk index based on the best-fit, exponential distribution, with mean of 1.98, sample size of 24, and 95% CI of (1.33, 2.96).

Focusing on a comparison between groups II (0.4 V/mil, 12.5 mil) and III (1.6 V/mil, 25 mil), it may be expected that an increase of electric field by four times would increase the risk index. However the mean of the risk index actually decreases. This suggests that the doubling of the spacing suppressed the increased risk resulting from the increase of the electric field by four times. The risk

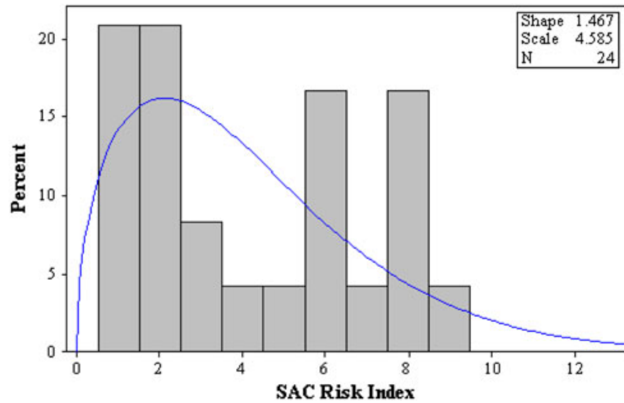

Fig. 17. Histogram of SAC risk index based on the best-fit, Weibull distribution, with mean of 4.15, sample size of 24, and 95% CI of (3.15, 5.47).

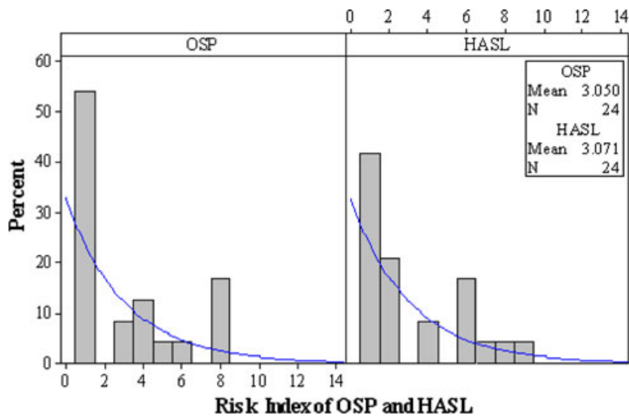

Fig. 18. Histogram of OSP and HASL risk index based on the best-fit, exponential distribution for both. OSP has mean of 3.05 and 95% confidence interval of (2.04, 4.55), and HASL has mean of 3.07 and 95% confidence interval of (2.06, 4.58). Sample sizes are both 24.

index decreased from 3.60 to 1.47, which implies a stronger and independent influence of spacing on risk, pointing to the importance of the path formation step in the ECM process.

Further exploration can be performed to clarify which factor—spacing or electric field—is more influential in determining the risk index, as shown in Fig. 19. Let asterisk "A" represent an imaginary group of 25 mil samples with 0.4 V/mil field. So, a transition from I → II can be viewed as I → A → II. The increase of risk index from group I (25 mil, 0.2 V/mil) to group III (25 mil, 1.6 V/mil) is 28%, so the transition from I to A (double the field) cannot increase the risk index by more than 28%. The transition from I to II (double the field and half the spacing) increased the mean of the risk index by 213%, thus suggesting that the transition from A to II (half the spacing) has potentially increased the risk index by 185%. Thus, under a relatively low electric field (less than 0.4 V/mil), a change of spacing by two times has a more significant effect on the risk index than a change of electric field by two times.

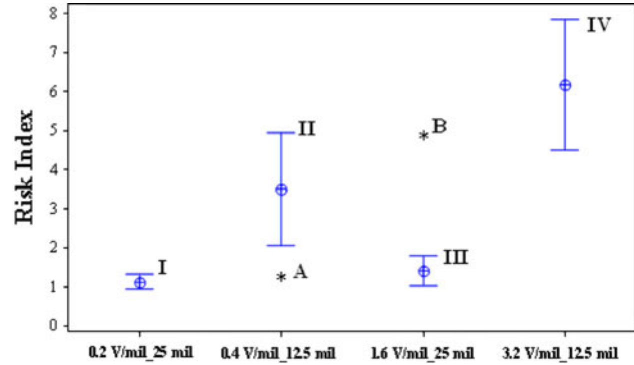

Fig. 19. Interval plot (95%) of risk index of four combinations of electric fields and their spacings. Group I (0.2 V/mil_25 mil) samples have mean of 1.15 and 95% confidence interval of (0.99, 1.35), group II (0.4 V/mil_12.5 mil) samples have mean of 3.60 and 95% confidence interval of (2.16, 5.04), group III (1.6 V/mil_25 mil) samples have mean of 1.47 and 95% confidence interval of (1.23, 1.91), and group IV (3.2 V/mil_12.5 mil) samples have mean of 6.41 and 95% confidence interval of (4.85, 7.96). The means and confidence intervals come from their best-fit distributions. Asterisk A and B are imaginary points to represent 0.4 V/mil_25 mil samples and 1.6 V/mil_12.5 mil samples, respectively.

Similarly, let asterisk "B" represent an imaginary group of 12.5 mil samples with 1.6 V/mil field. So, a transition from IV → III can be viewed as IV → B → III. The transition from IV to B (half the field) decreases the risk index by no more than 44%, which is the decrease of risk index from group IV to II (reduction of the field to one-eighth of the original value). However, the decrease of risk index from group IV to III (half the field and double the spacing) is 76%, so a change from B to III (double the spacing) can decrease the risk index by more than 32%. This implies that, under a relatively high field (higher than 1.6 V/mil), a change of spacing by two times is comparable to a change of electric field by two times in its effect on the risk index.

Together with the comparison between groups II and III discussed previously, it may be concluded that, when the electric field is less than 1.6 V/mil, spacing dominates the risk index, but when the electric field is larger than 1.6 V/mil, the electric field and spacing exert similar influence on the risk index.

CONCLUSIONS

IPC B-24 comb patterns have been tested under THB conditions to evaluate the propensity of eutectic SnPb and lead-free SAC solder to undergo ECM, and to assess the effects of board finish, electric field, and spacing. A clear relationship between the electrochemical behavior and electrical behavior of different solders was established. The dendritic growth on the surface led to intermittent SIR drops, metal layer deposition resulted in a long-term SIR decline, and the consumption of electroactive species generated the initial SIR increase right after humidity exposure, a characteristic of a

diffusion-controlled cell. A model based on 3D progressive and instantaneous nucleation was used to simulate the long-term SIR decline, and it matched the experimental data. The similarities between the simulation and experimental data indicate that both types of nucleation occurred.

This study shows that SAC solder can exhibit failures under THB conditions if there is a long-term incompatibility between the fluxes and solder systems. The failure mechanism for the SAC boards, the deposition of metallic layers, was different from the dendritic growth often encountered on SnPb boards. The long-term deposition of metallic layers on the SAC boards necessitates careful selection and evaluation of flux and solder systems to ensure their long-term compatibility. The SIR results obtained with SAC solder demonstrate that THB tests of 500 h or longer may be required to uncover reliability risks. SIR may exhibit a rising trend in the first 100 h to 200 h and give the impression of stabilization, whereas additional testing may reveal problems that could threaten the reliability of electronic products which have long expected lifetimes.

Comigration and codeposition of Sn, Pb, and Cu on the SnPb board and Sn, Cu, and Ag on the SAC board were observed. The codeposition of these metals was due to their low deposition potentials, which were in the millivolt range, compared with the 5 V or 40 V applied bias. Although it has been argued by some researchers that Ag cannot migrate at room temperature due to its formation of intermetallic compounds, a small amount of Ag migration was observed in some samples in this study on SAC boards. Among the migrated species, Sn was predominant and manifested itself as layer deposits, Pb was predominant in the dendrites, while only a small proportion of the migrated metal was Cu. The occurrence of dendrites on SnPb boards tested at 40 V rather than at 5 V was attributed to the larger chance for the cathodic overpotential to exceed the critical cathodic overpotential and trigger dendritic growth under conditions of higher electrical stress.

The occurrence of ECM was influenced less by surface finish than it was by solder alloy. In the case of OSP this was attributed to complexation of OSP during THB testing, which resulted in a nondetrimental green residue. In the case of HASL, the soldering process caused the HASL finish to dissolve into the solder, resulting in a final composition that was not sufficiently different from the nominal solder alloy composition to change its propensity for ECM compared with the OSP samples.

There was interaction between electric field and conductor spacing with respect to ECM. Within a spacing range from 12.5 mil (0.32 mm) to 25 mil (0.64 mm), when the electric field was relatively low (less than 1.6 V/mil), spacing was a stronger factor than electric field in affecting ECM. When the electric field was relatively high (larger than 1.6 V/mil), electric field had a comparable influence to spacing on ECM. With the current trend in the electronics industry towards miniaturization, higher-density products would be expected to have greater risk of ECM overall, and to exhibit greater sensitivity to spacing than to electric field. ECM's larger sensitivity to spacing implies that solely lessening the electric field may not be sufficient to mitigate risk, and additional measures are needed to effectively suppress ECM.

ACKNOWLEDGEMENTS

The authors would like to thank the more than 100 companies and organizations that support research activities at the Center for Advanced Life Cycle Engineering at the University of Maryland annually. The authors also express their appreciation to the members of the CALCE Electronic Products and Systems Consortium for providing test samples that were used in this study and for helpful discussions.

APPENDIX

Since Fickian diffusion is a special case of a general ion transport process, a series of ion transport equations can be introduced to give a general context in order to clarify the preconditions required for Fickian diffusion. This theoretical framework for ion transport is given by the Nernst–Planck equation,[17] which has broad applications in electrochemistry. The ionic flux J is

$$J = -D\frac{\partial c}{\partial x} - z\mu F c\frac{\partial \phi}{\partial x} + cV, \quad \text{(A1)}$$

where D is the diffusivity, c is the concentration, μ is the mobility of a specific type of ion, F is Faraday's constant, V is the hydrodynamic speed relative to the frame of the physical test setup, and z is the charge number of an ion. Here, V is zero, since the electrolyte is not stirred and static electrodes are used. When the bias is high (40 V or 5 V), c can be very small in the vicinity of the cathode and practically zero on the surface of the electrode.[17] Thus Eq. (A1) reduces to

$$J = -D\frac{\partial c}{\partial x}. \quad \text{(A2)}$$

Based on the continuity equation and assuming c_1 is an electroactive species in the electrolyte,

$$\frac{\partial c_1}{\partial t} \approx D_1\frac{\partial^2 c_1}{\partial x^2} \quad \text{(A3)}$$

with boundary conditions of

$c_1(x,0) = c_1^{\mathrm{b}}$ (initial bulk concentration at $t = 0$)

and

$c_1(x \to \infty, t) = c_1^{\mathrm{b}}$ (bulk concentration beyond the diffusion layer thickness).

Equation (A3) can be solved by Laplace transformation. Its final solution is

$$c_1(x,t) = c_1^{\mathrm{b}}\left(1 + (a-1)\mathrm{erfc}\left(\frac{x}{2\sqrt{D_1 t}}\right)\right),$$

where a is a constant related to the voltage step. So, the electric current density is

$$i_1(t) = z_1 F J_1 = -z_1 F D_1 \left(\frac{\partial c_1}{\partial x}\right)_{x=0} = z_1 F c_1^{\mathrm{b}}(a-1)\sqrt{\frac{D_1}{\pi t}}. \tag{A4}$$

If $c_1, c_2, \ldots, c_k, c_{k+1}, \ldots, c_n$ exist in the electrolyte, $c_1, c_2, \ldots, c_k$ are all the electroactive species, and $c_{k+1}, c_{k+2}, \ldots, c_n$ are all the electro-inactive species, then the electroneutrality assumption results in

$$\sum_1^n z_i c_i = 0.$$

Since Eq. (A4) can also apply to other electroactive species (not only c_1), the total current density is

$$\begin{aligned} i_{\mathrm{Total}} &= i_1(t) + i_2(t) + \cdots + i_k(t) \\ &= \sqrt{\frac{1}{t}} \cdot \sum_1^k \left(z_i F c_i^{\mathrm{b}}(a-1)\sqrt{\frac{D_i}{\pi}}\right). \end{aligned}$$

Thus, the resistance measured across the electrodes is

$$\begin{aligned} R = \frac{U}{i_{\mathrm{Total}} A} &= \frac{U}{\sqrt{\frac{1}{t}} \cdot \sum_1^k \left(z_i F c_i^{\mathrm{b}}(a-1)\sqrt{\frac{D_i}{\pi}}\right) A} \\ &= \frac{U}{\sum_1^k \left(z_i F c_i^{\mathrm{b}}(a-1)\sqrt{\frac{D_i}{\pi}}\right) A}\sqrt{t}, \end{aligned} \tag{A5}$$

where U is the voltage bias across the electrodes, and A is the cross-sectional area of the electrolyte.

REFERENCES

1. M. Pecht, E. Bumiller, D. Douthit, and J. Pecht, *Contamination of Electronic Assemblies* (Boca Raton, FL: CRC, 2003).
2. C. Lea, *A Scientific Guide to Surface Mount Technology* (Ayr, Scotland: Electrochemical, 1988).
3. C. Dominkovics and G. Harsanyi, *Microelectron. Reliab.* 48, 1628 (2008).
4. G. Harsanyi, *IEEE Trans. Compon. Packag. A* 18, 602 (1995).
5. R.C. Benson, B.M. Romenesko, J.A. Weiner, B.H. Nall, and H.K. Charles, *IEEE Trans. Compon. Hybr.* 11, 363 (1988).
6. D.Q. Yu, W. Jillek, and E. Schmitt, *J. Mater. Sci.: Mater. Electron.* 17, 229 (2006).
7. S.M. Ho, S.M. Lian, K.M. Chen, J.P. Pan, T.H. Wang, and A. Hung, *IEEE Trans. Compon. Packag. A* 19, 202 (1996).
8. A. Shumka and R. R. Piety, *Proc. Int. Reliab. Phys. Symp.* (Las Vegas, NV, 1975), p. 93.
9. Y. Awakuni and J. Calderwood, *J. Phys. D Appl. Phys.* 5, 1038 (1972).
10. B. Yan, S. Meilink, G. Warren, and P. Wynblatt, *IEEE Trans. Compon. Hybr.,* CHMT-10, 247 (1987).
11. L. Zou and C. Hunt, *J. Electrochem. Soc.* 156, C8 (2009).
12. S. Zhan, M.H. Azarian, and M. Pecht, *IEEE Trans. Electron. Packag. Manuf.* 29, 217 (2006).
13. IPC Publication IPC-TM-650, Method 2.6.14.1, *Electrochemical Migration Resistance Test* (Northbrook, IL: IPC, 2000).
14. D.Q. Yu, W. Jillek, and E. Schmitt, *J. Mater. Sci.: Mater. Electron.* 17, 219 (2006).
15. S. Zhan, M.H. Azarian, and M. Pecht, *Proc. 38th Int. Symp. Microelectron.* (Philadelphia, PA, 2005), p. 367.
16. Joint Industry Standard, IPC J-STD-004, *Requirements for Soldering Fluxes* (Northbrook, IL: IPC, 2004).
17. K. Kontturi, L. Murtomaki, and J. Manzanares, *Ionic Transport Processes in Electrochemistry and Membrane Science* (New York: Oxford University Press, 2008).
18. C.H. Hamann, A. Hamnett, and W. Vielstich, *Electrochemistry* (New York: Wiley–VCH, 1998).
19. K. Takahashi, *J. Electrochem. Soc.* 138, 1587 (1991).
20. M. Bendaoud, N. Bouchtout, F. Kaouah, and M. Saidi, *Proc. IEEE Int. Symp. Electr. Insul.* (Toroto, Canada, 1990), p. 199.
21. D. Das-Gupta, T. Welsh, and A. Goodings, *Proc. IEEE Dielect. Mater. Meas. Appl.* (Canterbury, UK, 1988), p. 258.
22. A. Saad and R. Tobazeon, *IEEE Trans. Electr. Insul.* EI-19, 193 (1984).
23. P. Atkinson and R. Fleming, *J. Phys. D Appl. Phys.* 9, 2027 (1976).
24. P. Atkinson and R. Fleming, *J. Phys. D Appl. Phys.* 13, 625 (1980).
25. T. Chapman and H. Wintle, *J. Appl. Phys.* 51, 4898 (1980).
26. M. Pepin and H. Wintle, *J. Appl. Phys.* 83, 5870 (1998).
27. D. Das-Gupta, *IEEE Trans. Electr. Insul.* 27, 909 (1992).
28. R.D. Armstrong, M. Fleischmann, and H.R. Thirsk, *J. Electroanal. Chem.* 11, 208 (1966).
29. E. Bosco and S.K. Rangarajan, *J. Electroanal. Chem.* 134, 213 (1982).
30. M.Y. Abyaneh, V. Saez, J. Gonzalez-Garcia, and T.J. Mason, *Electrochim. Acta* 55, 3572 (2010).
31. A. Sinni and M. Palmer, *Proc. IEEE/CPMT Int. Electron. Manuf. Tech. Symp*. (Austin, TX, 1997), p. 152.
32. S. Zhan, M.H. Azarian, and M. Pecht, *IEEE Trans. Dev. Mater. Reliab.* 8, 426 (2008).
33. J. Bradley, H. Chen, J. Crawford, J. Eckert, K. Ernazarova, T. Kurzeja, M. Lin, M. McGee, W. Nadler, and S. Stephens, *Nature* 389, 268 (1997).
34. IPC 9201A, *Surface Insulation Resistance Handbook* (Bannockburn, IL: IPC, 2007).
35. R. Pandey, S. Sahu, and S. Chandra, *Handbook of Semiconductor Electrodeposition* (New York, NY: Marcel Dekker, 1996).
36. P. Kohl, *J. Electrochem. Soc.* 129, 1196 (1982).
37. V. Maksimovic, M. Pavlovic, Lj. Pavlovic, M. Tomic, and V. Jovic, *Hydrometallurgy* 86, 22 (2007).
38. N. Nikolic, K. Popov, Lj. Pavlovic, and M. Pavlovic, *Surf. Coat. Technol.* 201, 560 (2006).
39. D. Dobos, *Electrochemical Data, A Handbook for Electrochemists in Industry and Universities* (Amsterdam, The Netherlands: Elsevier Scientific, 1975).
40. Y. Li, *Proc. IEEE/CPMT Int. Electron. Manuf. Tech. Symp.* (Austin, TX, 1997), p. 56.
41. E. Bradley and K. Banerji, *IEEE Trans. Compon. Packag. B* 19, 320 (1996).
42. E.C. Wagner and W.H. Millett, *Org. Synth.* 2, 65 (1943).
43. G. Mohamed, N. Ibrahim, and H. Attia, *Spectrochim. Acta A* 72, 610 (2009).
44. K. Tellefsen, *Proc. Int. Conf. Electron. Assem.: Mater. Process Challenges* (Atlanta, GA, 1998), p. 57.